Investigations of composite fermions in semiconductor nanostructures

1996 J. Phys.: Condens. Matter 8 3019

(http://iopscience.iop.org/0953-8984/8/17/013)

J. Phys.: Condens. Matter **8** (1996) 3019–3032. Printed in the UK

Investigations of composite fermions in semiconductor nanostructures

A Sachrajda†, Y Feng†, A Delage†, P Kelly†, H Carmona‡, P C Main‡ and L Eaves‡

† Institute for Microstructural Sciences, NRC, Ottawa, Canada K1A 0R6
‡ Department of Physics, University of Nottingham, Nottingham NG7 2RD, UK

Received 27 November 1995, in final form 26 February 1996

Abstract. We have measured the magnetoresistance of a variety of structures to search for effects associated with composite fermions (CF) near the Landau filling factor $\nu = 1/2$. We find evidence for effects due to randomization of semiclassical ballistic CF trajectories. These produce magnetoresistance features similar to those observed near zero magnetic field. However, we were not able to reproduce the recent CF magnetic focusing experiment despite using devices of very similar quality to those used in the original experiment. We also searched, without success, for phenomena due to phase coherence of CF. The relative ease with which the various magnetoresistance effects are seen in CF is discussed, in part with the aid of semiclassical simulations. It is discovered that inhomogeneities of carrier density cause the magnetoresistance anomalies to be smeared out, largely as a result of spatial variations in the effective magnetic field experienced by the CF. We find also that experiments which are based on randomization of trajectories are more resilient to this spatial variation.

1. Introduction

The fractional quantum Hall effect (FQHE) has recently been modelled in terms of a novel 'composite fermion' (CF) quasiparticle [1]. The CF comprises an electron bound to an even number of flux lines, each line carrying a flux quantum $\phi_0 = h/e$. The simplest CF occurs around the Landau filling factor, ν, equal to 1/2 (where $\nu = n\phi_0/B$ and B is the applied magnetic field) when the electron is bound to two flux quanta. Since the flux quanta are an integral part of the CF, the CF do not experience the magnetic field due to these flux lines. According to this theory, the CF experience an *effective* magnetic field given by

$$B^* = B \mp B_{1/2} \tag{1}$$

where $B_{1/2}$ is the applied magnetic field corresponding to $\nu = 1/2$, i.e. the magnetic field at which there are precisely two flux quanta for each electron in the system. Evidence for the existence of these quasiparticles has been provided by a number of experiments [2–4] performed in the CF regime. Some of these experiments showed evidence for the existence of semiclassical ballistic effects for the CF analogous to those well documented for electron gases at around $B = 0$. One experiment [3] measured magnetoresistance oscillations in a 2D antidot lattice which were attributed to a geometrical resonance between the period of the lattice and the cyclotron diameter of the CF moving in the effective field B^*. The oscillations were qualitatively (but not quantitatively) similar to those for electrons at around $B = 0$ but were of much weaker amplitude. Another principal experiment [4] showed a different

0953-8984/96/173019+14$19.50

magnetoresistance effect due to the magnetic focusing of CF between two constrictions. In this case, the CF effect was comparable in strength to that seen with electrons.

To the best of our knowledge, to date the two ballistic experiments have not been successfully reproduced in other laboratories [5] even where the equivalent electron effects are seen very clearly. This relative difficulty as regards the observation of ballistic phenomena in CF may be related to two differences between the electron and the CF regimes. First, it might be expected that the CF elastic mean free path ℓ would be shorter than the ($B = 0$) electron ℓ due to the larger CF effective mass [2]. This reduction in ℓ is consistent with the magnetoresistance experiments on the antidot lattice [3] but not with the magnetic focusing measurements [4]. Secondly, one needs to consider the role that intrinsic carrier density fluctuations play in the transport of ballistic particles. These inevitable fluctuations, of order 1%, affect electrons near zero magnetic field only via small changes in the Fermi wavevector $k_F \propto n^{1/2}$ which in turn lead to small variations in the cyclotron radius, $R_c = \hbar k_F/eB$, and hence small deviations from the 'average' ballistic trajectory. There are also small redirections of the trajectory due to the potential contours associated with the density fluctuations (i.e. the Snell's law analogue for electrons first discussed in the description of electron 'lens' experiments [6]). In the CF regime these effects are present too. However, the small density fluctuations also enter the CF cyclotron radius, $R_c^* = \hbar k_{CF}/eB^*$ (note that $k_{CF} = 2^{1/2}k_F$), through the equivalent spatial fluctuations in B^*. These effective magnetic field fluctuations can be very large, e.g. for a sample with $B_{1/2} = 10$ T, a 1% density variation would result in spatial variations of $B^* \sim 0.1$ T, which is comparable with a typical period for ballistic magnetoresistance features.

In this paper we report different types of measurement used to search for magnetoresistance effects due to CF. We note that ballistic magnetoresistance effects fall roughly into two categories: (a) those which rely on a geometric correspondence between the size of a semiclassical trajectory and some length scale of the device, e.g. simple magnetic focusing [7] and the bend resistance [8], and (b) those that are based on the randomization of these trajectories, e.g. the quenching of the Hall effect [9] and diffuse boundary scattering [10]. We call the former type G and the latter type R for future reference. We speculate that the latter category of effects will be more resilient to spatial fluctuations in B^*. In addition, for geometrical reasons ballistic effects in quantum wires and junctions require a smaller ℓ than those in the relatively open devices used in the previous CF experiments [3, 4]. On the basis of the above hypothesis one would expect that good candidates for observable ballistic CF magnetoresistance effects would be type R in quantum wires and junctions. It is also expected, however, that density fluctuations would be larger in smaller structures due to less efficient screening and the proximity of the device walls. We investigate this hypothesis experimentally by searching for both type G and type R effects and also by semiclassical modelling. We have also searched for magnetoresistance effects in the CF regime due to the phase coherence of the CF, although there are reasons why these phenomena may be very difficult to observe. In particular, fluctuations in B^* might be expected to affect weak localization due to the special role that zero magnetic field plays in this effect. Also, the thermal diffusion length will be much smaller for CF than for electrons due to the larger effective mass. The paper is set out as follows. In section 2 we describe the devices used and their fabrication. In section 3 we describe our experimental results obtained in searching for ballistic CF magnetoresistance effects of both G and R types. The experimental investigations of coherent effects in the CF regime are discussed in section 4. In section 5 we present the results of semiclassical simulations of some of the ballistic effects investigated, in the presence of a spatially fluctuating magnetic field. Section 6 contains the conclusions and suggestions for future work

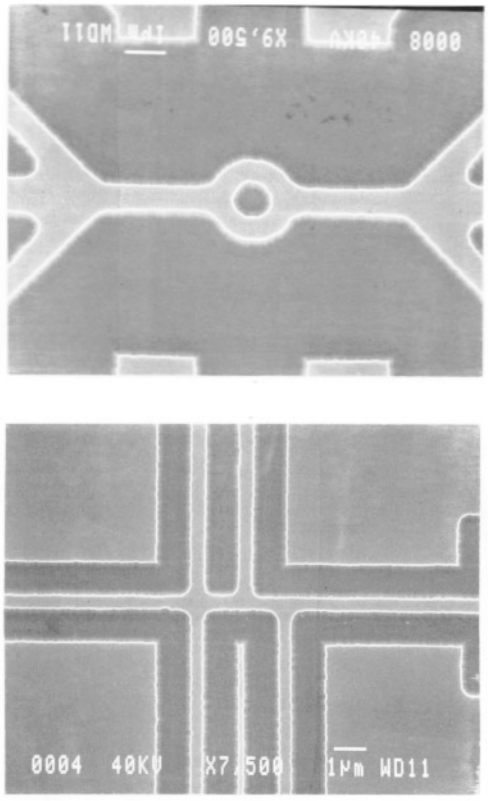

Figure 1. Electron micrographs of typical devices. Illustrated are a ring structure and a multi-probe wire.

2. Experimental devices

The devices were fabricated from high-mobility GaAs/(AlGa)As heterostructures grown by molecular beam epitaxy. The material used had an electron density between 0.7×10^{15} m^{-2} and 2×10^{15} m^{-2} with mobility in the range 200 to 400 m^2 V^{-1} s^{-1}. Three types of device were fabricated: quantum wires, quantum rings and parallel constrictions for focusing experiments. The wires and rings were fabricated using a shallow wet-etching technique. Investigations on a variety of test structures showed that this etching procedure produced the most reproducible and smallest edge depletion lengths (typically $\sim$0.15 μm). This property was considered important partly due the requirement for the width of the devices to be uniform. The relatively low electron density tends to lead to large depletion lengths. A variety of wires were fabricated with widths between 0.4 μm and 2 μm. The rings were all 1.5 μm in diameter, while the annular lithographic width was between 0.4 μm and 2 μm. After processing the quality of the material remained high, as illustrated by the observation of low-field Aharanov–Bohm oscillations in the magnetoresistance of the ring structures and also the FQHE at higher fields in all devices. Electron micrographs of two of these devices are shown in figure 1.

The parallel constrictions used in the magnetic focusing experiment were fabricated using standard electron beam lithographic techniques to manufacture gates on the surface of the heterostructure, as in the original experiment [4]. The characteristics of this device were found to be excellent in a variety of measurements. For example, measurements of the FQHE through the individual constrictions showed resistance plateaux corresponding

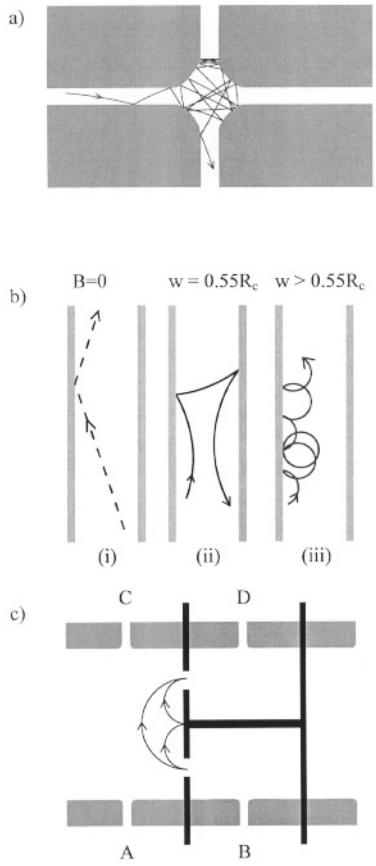

Figure 2. Schematic illustrations of three ballistic electron effects. (a) Scrambling of carrier trajectories in a cross structure which would lead to the quenching of the Hall resistance. (b) The diffuse scattering effect where an intermediate magnetic field ($w = 0.55R_c$) leads to an increase in the amount of boundary scattering and a peak in the magnetoresistance. (c) Carrier focusing. The thin lines represent the trajectories corresponding to the magnetic field where the first two magnetoresistance peaks occur.

to fractional filling factors with high denominators, e.g. 2/3, 3/5, 4/7 and 5/9 at magnetic fields below $\nu = 1/2$. This compares well with measurements of the FQHE on unprocessed material where the fraction with the highest denominator at magnetic fields below $\nu = 1/2$ was 7/13.

3. Experimental investigations of ballistic composite fermion effects

3.1. Ballistic magnetoresistance phenomena

Figure 2 illustrates schematically the origin of the principal magnetoresistance effects investigated in this section. All of them are well documented and understood [11] for the case of electron motion. Figure 2(a) represents the quenching of the Hall effect which can occur in cross structures with dimensions smaller than the mean free path. The phenomenon is a consequence of randomization of the carrier trajectories via scattering events at the junction boundaries. An electron injected from, say, the left-hand wire, as in figure 2(a), might normally be deflected towards the bottom probe by a magnetic field. However, the randomization of the trajectory means it has equal probability of entering either the top or bottom probe. Hence the Hall voltage, measured between these two probes, remains close to zero until the magnetic field is increased sufficiently for the carrier to enter the Hall probe without scattering off the walls, whereby the Hall voltage is established with the expected

sign. This effect falls into the R-type ballistic category defined above.

Figure 2(b) depicts the origin of the diffuse boundary scattering (DBS) effect first observed by Thornton *et al* [10]. In narrow wires or channels defined by etching or ion damage, as opposed to electrostatic gates, it is established that there is a significant probability of diffuse backscattering of the electrons at the wire boundaries. The left-hand diagram in figure 2(b) shows a typical ballistic trajectory in zero magnetic field. As B is increased, collisions with the walls become much more likely due to the deflection of the trajectories (centre diagram). This leads to the mean free path for backscattering decreasing with increasing magnetic field and hence a positive magnetoresistance. Eventually, however, as the magnetic field is raised still further and the cyclotron diameter becomes smaller than the wire width, as shown in panel (iii) of figure 2(b), the electron is guided along the edge of the wire even in the presence of diffuse scattering events. Hence there exists a field regime in which the mean free path increases with increasing magnetic field leading to a negative magnetoresistance. The overall effect then is that there is a positive magnetoresistance until $w/R_c = 0.55$ followed by a negative magnetoresistance. The magnetic field range of the DBS is very similar to that of the quenching of the Hall effect. We stress that the exact location along the wire where the diffuse boundary scattering occurs is not important as long as the average spacing between boundary scattering events leads to a mean free path having the field dependence described above. The DBS effect, therefore, also falls into the R category.

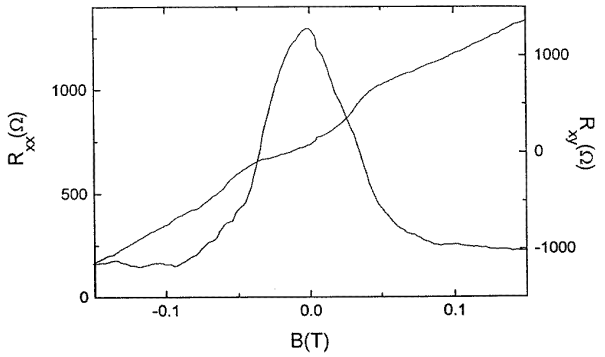

Figure 3. R_{xx} and R_{xy} at low magnetic fields and $T = 300$ mK for a wire junction (cf. figure 2(a)) of lithographed wire width 0.5 μm.

Figure 2(c) depicts a simple magnetic focusing experiment [7]. Ballistic electrons emerging from one constriction are steered by the magnetic field into the second constriction whenever the spacing between constrictions is an integer number of cyclotron diameters. If the contact behind the second constriction is used as a collector, its voltage shows a series of resonances with increasing B whenever the focusing criterion is obeyed. Adjacent resonances correspond to carrier trajectories which differ by one specular collision with the wall between the constrictions. We note that scattering on boundaries defined by electrostatic gates is largely specular. Spector *et al* [12] found that the mean free path relevant for this effect is smaller than that deduced from the mobility. Small-angle scattering has little effect on normal transport but in this experiment a small change in the trajectory may be enough to cause the carrier to miss the second constriction. This is clearly a G type of ballistic effect.

Note that all the ballistic effects described above scale in terms of the cyclotron radius

of the carriers. This gives an important comparison between the field scale of effects due to electrons and those due to CF in the same device. Because the CF are spin polarized, only one CF can occupy each $\boldsymbol{k}$-state and, since the density of CF at $\nu = 1/2$ is the same as the electron density, it follows that k_F for the CF is $2^{1/2}$ times larger than for electrons. The magnetic field scale for CF phenomena is therefore $2^{1/2}$ times larger than for electrons.

3.2. 'Type R' effects due to randomization of trajectories

The above effects were readily observable in our devices for electrons near $B = 0$. For example, figure 3 shows the longitudinal resistance (R_{xx}) of a section of wire with lithographic width 0.5 μm and also the Hall resistance (R_{xy}) at a junction. The quenching of the Hall resistance is clearly visible in R_{xy}. The peak in R_{xx} is not simply due to the DBS effect, which should show a peak in resistance at finite field. We believe that there is an extra contribution to the resistance at $B = 0$ due to a phase-coherent effect related to weak localization; this is discussed in more detail below. Such effects have been seen in a number of mesoscopic structures [13]. The magnetic field scale over which the DBS and the quenching of the Hall resistance occur is consistent with the scaling law above, within the uncertainties of the widths of our wires due to edge depletion.

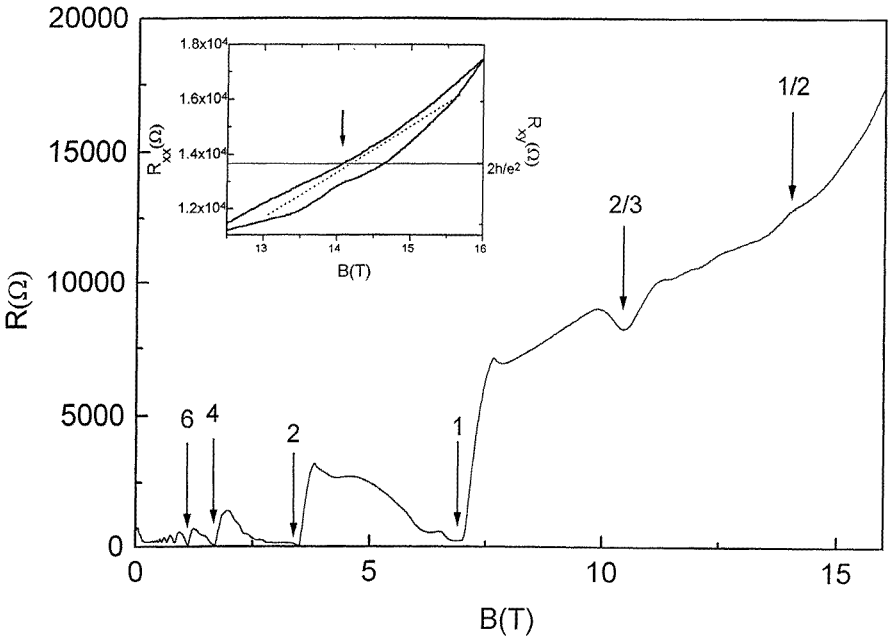

Figure 4. R_{xx} from $B = 0$ T to $B = 15$ T at $T = 1.2$ K for a wire of lithographic width 0.5 μm. The inset shows R_{xx} (lower) and R_{xy} (upper) for the same wire in detail at around $\nu = 1/2$. The dashed straight line is a guide. The sample geometry is similar to that shown in figure 2(a).

Figure 4 shows the longitudinal magnetoresistance, R_{xx}, at 1.2 K from 0 to 15 T of a quantum wire of lithographic width 0.5 μm. At this temperature the FQHE is barely visible and only a weak dip is seen in the trace at $\nu = 2/3$. At $\nu = 1/2$, there is a small but clearly defined *peak* in the resistance. This is in contrast to the weak *dip* which is

observed at $\nu = 1/2$ in the magnetoresistance of bulk samples [14]. This peak is common to most of our narrow samples and we tentatively associate it with the CF version of the magnetoresistance feature near $B = 0$ shown in figure 3. However, the peak is so weak and ill-resolved that no detailed comparison of the two features can be made. In the inset of figure 4, R_{xx} is shown a little more clearly with $n = 1/2$ arrowed. The width of the peak is slightly larger than that predicted from scaling by $2^{1/2}$ the width of the peak in figure 3, perhaps due to variations in B^*. Also shown in the inset to figure 4 is the Hall resistance of a junction. There is evidence for an extremely weak quenching effect in the Hall resistance at $\nu = 1/2$ as indicated by the departure of R_{xy} from the straight dotted line which is included as a guide to the eye.

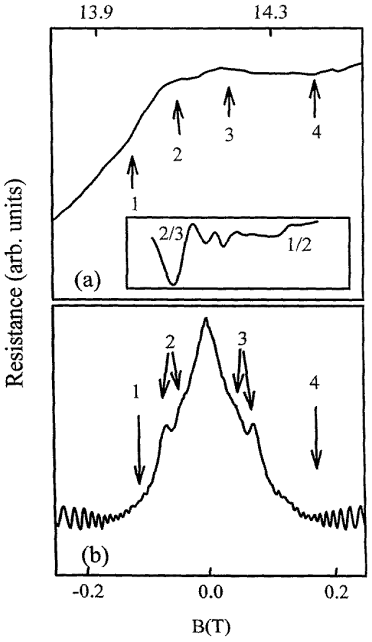

Figure 5. Longitudinal resistance R_{xx} at $T = 300$ mK of a wire of lithographic width 0.5 μm (a) in the vicinity of $\nu = 1/2$ and (b) around $B = 0$. The B-axis in (a) has been scaled to be comparable with that in (b). The arrowed features are described in the text. The inset to (a) shows R_{xx} over a wider range of B from $\nu = 2/3$ to $\nu = 1/2$. The sample geometry is as shown in figure 2(a).

In some devices, the peak at $\nu = 1/2$ contains a richer structure which is not resolved in figure 4. Figure 5(b) shows the magnetoresistance at around $B \sim 0$ for a wire of width 0.5 μm at 300 mK. The equivalent magnetoresistance at around $\nu = 1/2$ (i.e. $B = 14.12$ T) is shown in figure 5(a) with the magnetic field axis scaled by $2^{1/2}$ to allow a direct comparison of the respective field scales. The inset shows the same measurement over a wider field range. The extent of the broad magnetoresistance peak at around $B = 0$, depicted as points 1 and 4 in figure 5(b), scales very neatly with its extent in figure 5(a), also labelled as points 1 and 4. Also, features 2 and 3, which we associate with the DBS effect, are also reproduced in figure 5(a) in the correct scaled positions. However, whereas figure 5(b) is dominated by the weak-localization feature at $B = 0$, this is entirely absent from figure 5(a). Instead there is a weak dip precisely at $\nu = 1/2$ which is exactly what we would expect in the magnetoresistance due to a pure DBS effect and what we would also have expected to have seen at $B = 0$ in the absence of the central weak-localization peak (see section 4 for a discussion of phase-coherence effects in CF).

It is clear that the magnetoresistance behaviour at around $\nu = 1/2$ is different in quantum wires from that in the bulk. These differences in behaviour are consistent with the presence

of ballistic effects in CF but do not constitute definite proof of their existence since the effects are weak and device dependent (for example, the structure in figure 5 is much better resolved than that in figure 4).

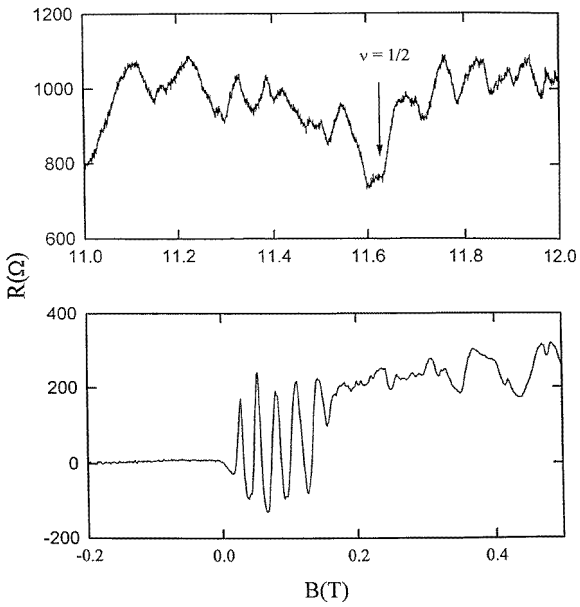

Figure 6. Magnetic focusing peaks in magnetoresistance in the vicinity of $B = 0$ (lower) and in the vicinity of $\nu = 1/2$ (upper). The sample details are given in the text. The magnetic field axis has been scaled by $2^{1/2}$ in the upper diagram to allow direct comparison. Referring to figure 2(c), current is passed from contacts A to B and voltage is measured between C and D.

3.3. Magnetic focusing ('type G')

We turn now to our attempts to observe the magnetic focusing effect in the CF regime. The device configuration is shown schematically in figure 2(c). Current is passed between contacts A and B and the voltage is measured between contacts C and D. An advantage of this configuration is that the measured voltage is close to zero except where focusing occurs. The device characteristics (constriction widths 0.5 μm, separation 4.5 μm, electron density 1.1×10^{15} m^{-2}, mobility in the dark 250 m^2 V^{-1} s^{-1}) were chosen to be as close as possible to the parameters of the original CF focusing experiment [4]. The lower curve of figure 6 shows the measured resistance versus B around $B = 0$. Clear focusing peaks can be seen for $B > 0$, with a period consistent with the density and constriction spacing. The total number of peaks observed is also in line with the constriction width. The upper curve shows the equivalent trace in the vicinity of $\nu = 1/2$ with the magnetic field axis scaled by $2^{1/2}$ to allow direct comparison of the curves. Although there are clear, reproducible fluctuations in the resistance over a wide field range, similar to those reported in [4], we were not able to identify any behaviour asymmetric with respect to $\nu = 1/2$. A similar lack of evidence for focusing was observed when we reversed the direction of the applied magnetic field and also after the mobility was raised by illumination to around 400 m^2 V^{-1} s^{-1}.

To summarize our major observations from the ballistic experiments, our data are consistent with the observation of the DBS effect in narrow wires in the CF regime and,

in addition, we have some preliminary evidence for the quenching of the Hall resistance at around $\nu = 1/2$ in small junctions. However, we have not been able to reproduce magnetic focusing of CF in our devices, even though the magnetoresistance peaks were very strong at around $B = 0$.

4. The experimental search for phase coherence in CF

In this section we discuss three magnetoresistance effects associated with the phase coherence of the carriers: weak localization, Aharonov–Bohm oscillations and universal conductance fluctuations. Weak localization [15] occurs as a result of the interference between time-reversed trajectories around the same spatial path and is usually a feature of disordered material. As such, there is very little evidence of weak localization in our high-mobility bulk material. However, in mesoscopic wires and junctions, there may be trajectories associated with the device boundaries which can lead to interference between time-reversed paths analogous to weak localization [13].

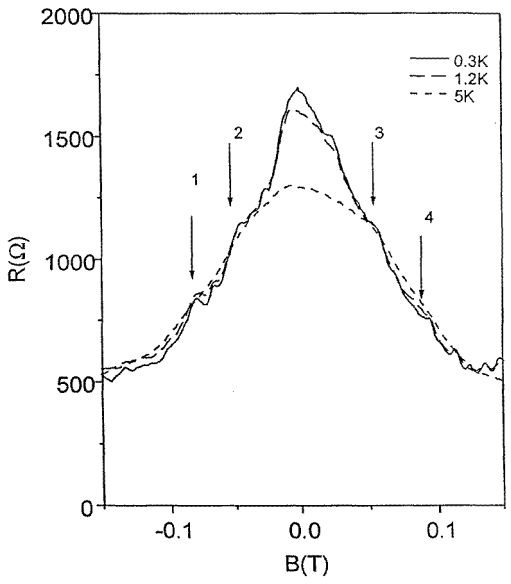

Figure 7. Magnetoresistance peaks at around $B = 0$ for a wire of width 0.5 μm at three temperatures.

Evidence for the presence of weak localization in our structures is shown in figure 7. This shows the magnetoresistance at around $B = 0$ of a wire of lithographic width 0.5 μm at three different temperatures. The low-field resistivity changes with temperature and so the three curves have been offset so that the feature labelled '1' has an identical resistance in all three cases. It is clear that the central region of the peak has a more rapid temperature dependence than the rest of the feature. We attribute this to a weak-localization contribution near zero field. We believe that it masks the expected dip in resistance at zero field associated with the DBS effect.

The weak-localization feature is expected to be absent in the CF regime near $\nu = 1/2$ for a fundamental reason. Weak localization reflects the breaking of time-reversal symmetry by a magnetic field. At zero field, the time-reversed trajectories are exactly in phase regardless of the interference path length. Thus a consistent definition of zero magnetic field is crucial for weak localization. In the electron case, there is no problem with this since the

magnetic field is applied externally. However, in the CF case where the definition of B^* depends on the carrier concentration, electron density fluctuations cause spatial modulations in the effective magnetic field. In particular, B^* is zero at different applied magnetic fields in different parts of the sample. Nevertheless, it may still be possible to observe weak localization provided that this variation in B^* is less than the equivalent of one flux quantum threading the largest phase-coherent loop in the device. For a phase-coherent loop of ~ 1 μm diameter this would require a spatial homogeneity in the electron density of $\sim 0.1\%$ which is rather better than is routinely achieved. Hence, we would expect the weak-localization peak to be absent in the CF regime. Figure 5 shows evidence for this as discussed in section 3.2. Figure 5, therefore, not only reinforces our earlier observations of the presence of ballistic magnetoresistance effects near $\nu = 1/2$, it also illustrates that interference due to time-reversed paths of CF is very difficult to observe due to inhomogeneities in carrier density.

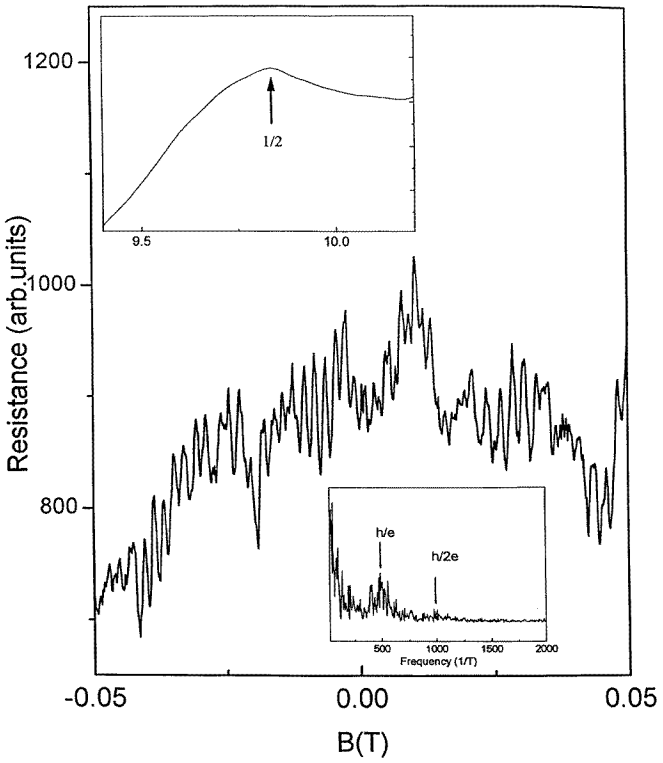

Figure 8. The magnetoresistance of a loop 1.5 μm in diameter with wire width 0.7 μm at $T = 300$ mK. The lower inset shows the Fourier transform of the main trace and the upper inset shows the magnetoresistance of the same sample at around $\nu = 1/2$.

The Aharonov–Bohm (AB) effect, which has previously been observed by several authors near $B = 0$ in semiconductor rings [16], does not have the extreme sensitivity to the definition of $B = 0$ since it does not necessarily involve time-reversed trajectories. Figure 8 shows the magnetoresistance near $B = 0$ at $T = 300$ mK of a ring of diameter 1.5 μm and wire width 0.7 μm. There are clear AB oscillations with amplitude $\sim 0.05e^2/h$ and period (see the lower inset for the Fourier transform) consistent with the area of the

ring. The upper inset shows the same measurement at around $\nu = 1/2$. Although, as usual, we see a peak at $\nu = 1/2$ due to ballistic effects (this has been subtracted from the data in the main figure for clarity) there is no sign of AB oscillations. Whether it is possible in principle to observe the AB effect in CF is not clear. However, in our experiment it is likely that, even at 300 mK, the effect would be thermally smeared. The CF effective mass is $\sim$10 times larger than that of a normal 2D electron. This means that the diffusion constant, D, is nearly two orders of magnitude smaller for CF than for electrons. It follows that the thermal diffusion length, $L_T = (\hbar D/k_B T)^{1/2}$, which provides a maximum length scale on which the AB effect may be observed, is about ten times smaller for CF than for electrons at the same temperature. For the measurement temperature of figure 8, L_T may be only $\sim$100 nm for CF, which is very much smaller than the perimeter of the ring. Evidently, very small devices are going to be required, or very low temperatures, if the AB effect is to be observed in CF.

Similar remarks may also apply to universal conductance fluctuations (UCF) [17]. Again, L_T determines the maximum size of a sample which will allow UCF to be seen. However, since the observation of UCF requires only a narrow wire and not a multiply connected device as in the AB experiment, they are more plausible candidates for the observation of phase-coherent effects. Unfortunately, the high-mobility 2D gases required for the observation of CF effects are not the best systems for looking at UCF. We do see reproducible UCF near $B = 0$ in our devices—for example the envelope of the AB oscillations in figure 8—but these are not reproduced near $\nu = 1/2$, not least because the device is very much longer than L_T. It is interesting to note that reproducible resistance fluctuations are seen near $\nu = 1/2$ in the experiment which attempted to see CF magnetic focusing (see figure 6). The problem is that it is very difficult to assign these fluctuations unambiguously to interference of the CF since similar fluctuations are well known in the *electron* edge state regime in mesoscopic devices [18]. However, if we were to assign these fluctuations to UCF in the CF, and further assume that it is the geometrical constrictions (see figure 2(c)) which have the largest resistance, then the phase-coherent subunit would have a size $\sim$100 nm which is in line with our earlier estimates.

5. Simulations of ballistic effects

The hypothesis that some types of ballistic magnetoresistance effect (R type) are less sensitive to spatial fluctuations of the (effective) magnetic field than others (G type) is supported by our experimental results. To explore this further, we have performed simulations of two ballistic experiments, one type R and one type G, in the presence of carrier density inhomogeneities. The inhomogeneous potential enters the calculations in several ways. First, the potential contours associated with the inhomogeneity guide the carriers at the Fermi energy due to the spatial dependence of the Fermi speed. Secondly, the spatial variation of k_F also means that the cyclotron radius, or curvature of the trajectory in a magnetic field, is spatially dependent, even in a completely homogeneous magnetic field. These two effects, which apply as much to electrons as to CF, were found to be insignificant for the range of inhomogeneities considered here. However, the third consequence, the spatial variation of B^* which is only relevant in the CF case, has a large effect on the simulations.

For the simulations of the density fluctuations, the section of the 2DEG was split conceptually into a grid. To describe the magnetic focusing experiment (type G) we used 50×50 square cells to represent a 5.5 μm $\times$ 5.5 μm square of material. Each cell was assigned a random number between zero and one except the cells at the edge of the square

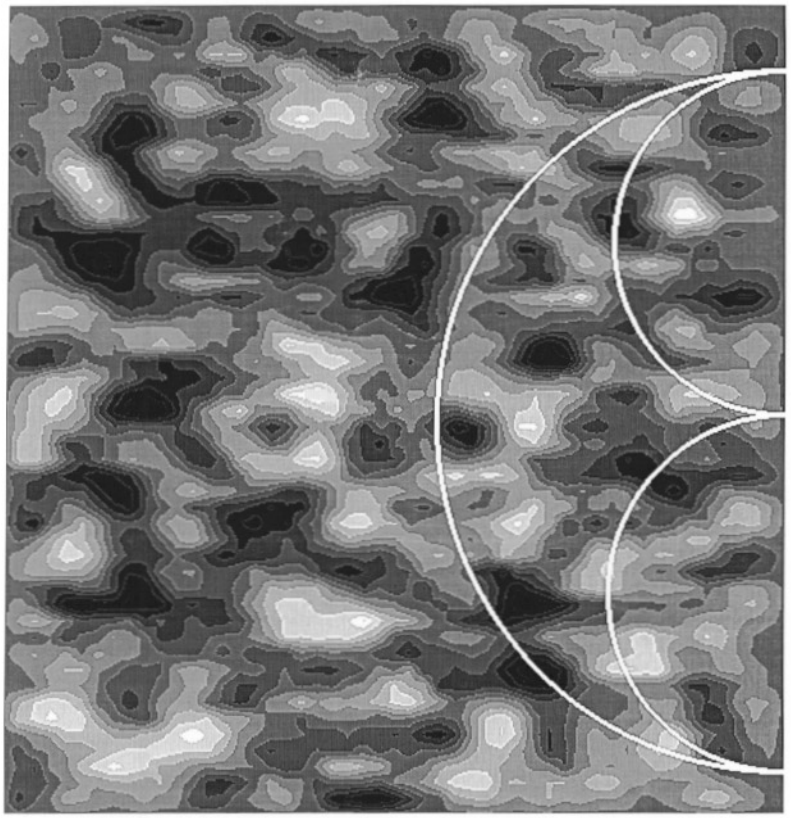

Figure 9. A typical smoothed random density profile with black and white representing the minimum and maximum densities respectively. White lines show typical trajectories in a focusing experiment (cf. figure 2(c)).

which were fixed at 1/2. We then smoothed this distribution by assigning to each cell a number which was the mean of its original value and those of its four nearest neighbours. This procedure was repeated three more times. Then, the mean number over the whole sample was set equal to the measured electron density, n, in the experiment and the variation of this mean was set to be $\pm\delta n$ where δn is the chosen percentage variation of n. A typical profile of n resulting from such a simulation is shown in figure 9 in a grey-scale plot. Also shown in figure 9 are some typical magnetic focusing trajectories as they would occur in the absence of potential fluctuations. A full analysis of the semiclassical trajectories for composite fermions was performed with an injection cone angle of 50° and a mean free path in excess of 6 μm. Figure 10 shows how the corresponding peaks in the magnetoresistance degrade as δn is increased. At $\delta n = 3\%$ the peaks have essentially disappeared. In this simulation it appears that the random variations in B^* are responsible for the degradation of the peaks. Refraction effects due to abrupt density changes from one cell to another are of minor consequence in the results of the simulation.

For the R-type simulations, the variations in B^* appear to have a much weaker effect as we suggested above. For example, 20×200 cells were used to represent a 0.6 μm $\times$ 6 μm wire. The density profile, after the smoothing procedure, is similar to a thin slice of figure 9. We simulated the boundary scattering effect [10] by using an injection cone of

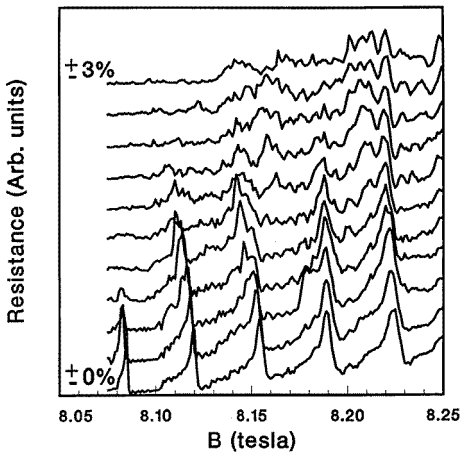

Figure 10. The destruction of the magnetic focusing peaks in the simulated magnetoresistance of composite fermions as the amplitude of the density fluctuations is increased from 0 to ±3%. Curves are offset for clarity.

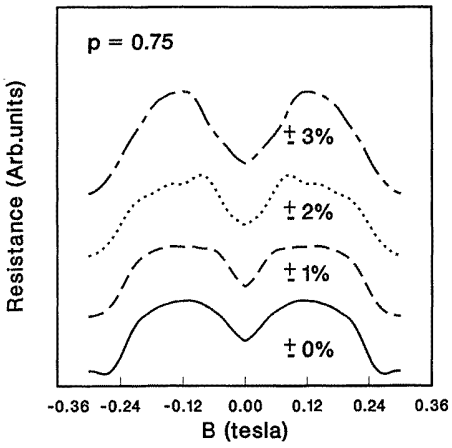

Figure 11. The effect of density fluctuations on the diffuse boundary scattering magnetoresistance of composite fermions (see the text for details). Note the resilience of the peaks with respect to increasing disorder relative to the focusing peaks in figure 10.

90° and performing a semiclassical analysis of the trajectories. Diffuse boundary scattering was incorporated by generating a random number, r, between 0 and 1 for each scattering event. If r were less than the chosen specular parameter, p, the reflection was considered specular. For $r > p$, the reflection was allowed to occur at an angle $\pi(1-r)/(1-p)$ with respect to the axis of the wire. Carriers were taken as transmitted or reflected according to which end of the wire they emerged from; the small number which were trapped in the wire were assigned 50% transmission probability. Repeated runs of the simulation indicate that we have ±10% uncertainty in the results. Results for a typical simulation of the magnetoresistance in a wire for $p = 0.75$ are shown in figure 11. The well-known magnetoresistance peak is apparent for CF as with electrons. However, in contrast to what was found in the simulation of the magnetic focusing effect, the peaks are robust against density variations of up to 3%. Again, the major contribution to the quenching of the peaks is the spatial variation of B^*.

6. Conclusions

In conclusion, we have carried out a comprehensive search for magnetoresistance effects associated with the semiclassical ballistic motion of CF, together with a preliminary investigation of phenomena associated with their phase coherence. We are unable to reproduce the magnetic focusing experiment described in [4] despite using devices with characteristics very similar to those of the original ones. However, we do find some evidence at around $\nu = 1/2$ for the existence of magnetoresistance anomalies associated with scrambling of ballistic trajectories, indicating that this sort of effect may be easier to observe than those which rely on the properties of a single, long trajectory. Numerical simulations of the semiclassical motion of carriers in an inhomogeneous potential corroborate this observation and indicate, for example, that the successful observation of magnetic focusing peaks requires carrier density homogeneities of better than 1% over the length of the

trajectories.

The observation of phase-coherent phenomena in CF appears a very difficult task requiring very low temperatures and very small devices. Weak-localization-type phenomena which depend on time-reversed trajectories having zero phase difference at $B = 0$ are very susceptible to spatial variations of B^*. Observation of AB oscillations will require very small devices, probably ∼100 nm diameter rings, because all the relevant length scales depend on the square root of the diffusion constant which is around 100 times smaller for CF than for electrons with the same scattering rate. Perhaps the best candidate for the observation of a phase-coherent effect is the study of UCF which requires relatively simple devices which can be made very small. A successful demonstration of composite fermion UCF will require rather more than the observation of magnetoresistance fluctuations near $\nu = 1/2$. To be convincing it will need a full temperature dependence of the amplitude and correlation field [16] in a set of devices of different dimensions [19].

Acknowledgments

This work was supported by the EPSRC (UK) and the EU-financed ECAMI project. HAC and LE are grateful to CNPq (Brazil) and the Royal Society respectively for financial support.

References

[1] Jain J K 1989 *Phys. Rev. Lett.* **63** 199
Lopez A and Fradkin E 1991 *Phys. Rev.* B **44** 5246
Halperin B I, Lee P A and Read N 1993 *Phys. Rev.* B **47** 7312
[2] Willet R L, Ruel R R, West K W and Pfeiffer L N 1993 *Phys. Rev. Lett.* **71** 3846
[3] Kang W, Stromer H L, Pfeiffer L N, Baldwin K W and West K W 1993 *Phys. Rev. Lett.* **71** 3850
[4] Goldman V J, Su B and Jain J K 1994 *Phys. Rev. Lett.* **72** 2065
[5] Weiss D 1995 private communication
At the recent EP2DSXI Conference in Nottingham there were several other similar observations reported privately.
[6] Sivan U, Heiblum M, Umbach C P and Shtrikman H 1990 *Phys. Rev.* B **41** 7937
See also [12].
[7] van Houten H, Beenakker C W, Williamson J G, Broekaart M E I and van Loosdrecht P H M 1989 *Phys. Rev.* B **39** 8556
[8] Timp G, Behringer R, Sampere S, Cunningham J E and Howard R E 1989 *Nanostructure Physics and Fabrication* ed M Reed and W P Kirk (New York: Academic)
[9] See, for example,
Ford C J B, Washburn S, Büttiker M, Knoedler C M and Hong J M 1989 *Phys. Rev. Lett.* **62** 2724
[10] Thornton T J, Roukes M L, Scherer A and Vandegaag B P 1989 *Phys. Rev. Lett.* **63** 2128
[11] Beenakker C W J and van Houten H 1991 *Solid State Physics* vol 44, ed H Ehrenreich and D Turnbull (New York: Academic)
[12] Spector J, Stormer H L, Baldwin K W, Pfeiffer L N and West K W 1990 *Appl. Phys. Lett.* **56** 1290
[13] Chang A M, Baranger H U, Pfeiffer L N and West K W 1994 *Phys. Rev. Lett.* **73** 2111
[14] Jiang H W, Stormer H L, Tsui D C, Pfeiffer L N and West K W 1989 *Phys. Rev.* B **40** 12 013
[15] Abrahams E, Anderson P W, Licciardello D C and Ramakrishnan T V 1979 *Phys. Rev. Lett.* **42** 673
[16] Timp G, Chang A M, Cunningham J E, Chang T Y, Mankiewich P, Behringer R and Howard R E 1987 *Phys. Rev. Lett.* **58** 2814
[17] Al'tshuler B 1985 *Pis. Zh. Eksp. Teor. Fiz.* **41** 530 (Engl. Transl. 1985 *JETP Lett.* **41** 648)
Lee P A and Stone A D 1985 *Phys. Rev. Lett.* **55** 1622
[18] Timp G, Mankiewich P, Devegvar P, Behringer R, Cunningham J E, Howard R E, Baranger H U and Jain J K 1989 *Phys. Rev.* B **39** 6227
[19] Lee P A, Stone A D and Fukuyama H 1987 *Phys. Rev.* B **35** 1039